Article

Experimental Investigation on the Laminar Flame Velocities and Markstein Lengths of Methane and PRF95 Dual Fuels

Sotiris Petrakides, Rui Chen, Dongzhi Gao, and Haiqiao Wei

Energy Fuels, **Just Accepted Manuscript** • DOI: 10.1021/acs.energyfuels.6b00644 • Publication Date (Web): 01 Jul 2016

Experimental Investigation on the Laminar Flame Velocities and Markstein Lengths of Methane and PRF95 Dual Fuels

Sotiris Petrakides [a], Rui Chen [a,*], Dongzhi Gao [b], Haiqiao Wei [b]

[a] Department of Aeronautical and Automotive Engineering, Loughborough University, LE11 3TU, United Kingdom

[b] Sate Key Laboratory of Engines (SKLE), Tianjin University, Tianjin 300072, China

[*] Corresponding author.

E-mail address: r.chen@lboro.ac.uk

Abstract

Natural gas is a promising alternative fuel. The main constituent of natural gas is methane. The slow burning velocity of methane poses significant challenges for its utilization in future energy efficient combustion applications. The effects of methane addition to PRF95 on the fundamental combustion parameters, laminar flame velocity (S_u^0) and Markstein length (L_b), were experimentally investigated in a cylindrical combustion vessel at equivalence ratios of 0.8,1,1.2 , initial pressures of 2.5, 5, 10 Bar and a constant temperature of 373 K. Methane was added to PRF95 in three different energy ratios 25%, 50% and 75%. Spherically expanding flames were used to derive the flow corrected burning velocities, from which the corresponding L_b and S_u^0 were obtained. The burning velocities were corrected for the motion of burned gas induced by the cylindrical confinement. It has been found that at stoichiometric conditions there is a linear decrease in L_b and S_u^0 with the DF ratio in all investigated pressures. At rich conditions, all DFs resulted to have lower S_u^0 as compared to methane and to a larger extend PRF95. The values of L_b for all DFs were lower than methane and comparable to those of PRF95. At lean conditions, the values of L_b for all DFs are biased towards those of methane whereas the values of S_u^0 found to be higher than those of PRF95 at pressures of 2.5 and 5Bar. At 10 Bar both L_b and S_u^0 reduce with DF ratio although S_u^0 of all DFs coverage to that of PRF95. The findings of the current study indicate a distinct synergy in the utilization of dual fuelling in future lean burn energy efficient combustion applications.

Keywords: *Natural gas, Gasoline, Dual fuel, Combustion characteristics, Laminar flame velocity, Markstein length.*

1. Introduction

Environmental impact of greenhouse gas emissions, as well as future air quality, are forcing governmental bodies to continuously update their legislations, adopting challenging emission standards. The necessity for compliance with future emission legislations has renewed the interest for the use of alternative fuels. The low carbon content and the abundance reserves, have classified natural gas as one of the most promising alternative fuels. The major constituent of natural gas is methane. Historically, the slow burning velocity of methane has been a major concern for its utilisation in energy efficient combustion applications *(1,2)*. The slow burning speed degrades the thermal efficiency of an SI engine and it is a contributor for hydrocarbon emissions. It is well acknowledged that the impact of methane hydrocarbon emissions on the greenhouse effect is considerably higher than the impact of CO_2.

A large body of literature has examined the binary blending of hydrogen with methane as an effective measure of increasing methane's burning velocity, and extending its lean burn limits *(3,4,5)*. Although from a purely combustion prospective the results are positive, the lack of mature hydrogen infrastructure is mainly preventing the global adaptation of this technology in the short to medium term.

As emphasized in literature on experimental studies in SI engines *(6 7,8)*, the addition of gasoline to methane (Methane-Gasoline Dual Fuelling) has also the potential to improve methane's combustion, leading to an enhanced initial establishment of burning velocity even compared to that of gasoline.

Practical combustion phenomena, including burning velocity in SI engines, are governed by the fundamental laminar flame velocity (S_u^0) of the fuel-oxidizer mixture. Since all realistic flames are curved and/or travel through a strained flow field, another fundamental mixture parameter known as the Markstein length (L_b), which quantifies the response of the flame velocity to stretch rate, is also necessary to characterise flame behaviour more completely *(9)*. A comprehensive understanding of these two fundamental mixture parameters $S_u^0$and L_b, is essential for the development of energy efficient combustion applications.

Substantial efforts have been devoted for improving the understanding on methane as well as gasoline combustion. Typical refinery gasoline consists of hundreds of hydrocarbons. Iso-octane as well as binary blends of primary reference fuels have been widely adopted as convenient gasoline surrogates. Studies reporting values of laminar flame velocities at elevated pressures have been conducted for gasoline *(10,11)* and its surrogates (*11,12,13,14)* as well as methane (*15,16,17)*. In all the above studies the reported laminar flame velocity of methane is consistently lower compared to that of gasoline and its surrogates when tested at similar conditions. Measured values of Markstein length have been reported for iso-octane and methane air mixtures *(12,15,16,18)*. A part of the study of Gu et al. (*15)* and Mandilas et al. (*18)* compared the Markstein length of iso-octane and methane air mixtures at different equivalence ratios. As emphasized, these two fuels responded to flame stretch in an opposite manner with respect to the equivalence ratio. The Markstein length of iso-octane increases with

equivalence ratio whereas that of methane decreases. At lean conditions, methane has a significantly lower Markstein length compared to iso-octane.

It appears that there is limited prior experimental work reporting the fundamental combustion parameters, laminar flame velocity and Markstein length, of a methane-gasoline dual fuel blend. The authors are only aware about the recent study of Baloo et al. (*19)* reporting the laminar flame velocities and Markstein lengths of methane-isooctane dual fuels at various equivalence ratios. The experiments have been conducted at atmospheric pressure, and a temperature of 363 K. It has been reported that the addition of methane to iso-octane increases both the laminar flame velocity as well as the stretched burning velocity in lean conditions but decreases both velocities in the rich conditions.

The laminar flame velocity and Markstein length of methane-gasoline dual fuels need further investigation especially at elevated pressures. It is therefore the aim of this study to experimentally investigate the relationship between laminar flame velocity and Markstein length, with the ratio of gas to liquid in a dual fuel blend at elevated pressures. In the current experimental work a binary blend of primary reference fuels commonly known as PRF95 (95%vol_{liq} of iso-octane and 5%vol_{liq} n-heptane) was used as the liquid fuel. Methane was used as the gaseous fuel. Values of laminar flame velocities and Markstein lengths are measured at equivalence ratios of 0.8, 1, 1.2, initial pressures of 2.5, 5, 10 Bar and a temperature of 373 K.

2. Experimental Technique

2.1 System Integration

A 100mm inner diameter cylindrical combustion vessel with a volume of 2.2L was employed for the experimental study. The experimental setup is illustrated in Figure 1. Optical access was possible through two opposing 80mm circular windows attached near the side of the bomb. The entire bomb was uniformly preheated by a set of electrical heating elements totaling 3.2-kW. One of the heaters was fully inserted inside the vessel to induce a transient temperature difference only during the filling process. The temperature difference evoked natural convection to stir the mixture enhancing the mixing of fuel and air. Similar technique has been used by Jerzembeck et al. *(11)*. The interior air temperature was controlled within 3 K using a closed-loop feedback controller set to 373K. The temperature could also be observed manually from a second temperature sensor mounted on the top of the bomb. The pressure rise during the combustion process was obtained using a Kistler 6113B pressure transducer. The mixture was ignited using a slightly modified standard ignition plug with extended electrodes of 1.35mm in diameter. The ignition system generated a spark with duration of 0.7 ms. For safety reasons, a 6 MPa pressure release valve was installed on the combustion vessel.

The flame progress recorded at 6000 frames per second with a resolution of 512X512 pixels by high speed schlieren photography arranged in a Z configuration. A 245W lamp was used as the light source. The light was focused onto a slit using a focusing lens in order to generate the spotlight for the schlieren technique. Passing through a group of mirrors, the light path was then cut by a knife-edge which is essential for the schlieren method *(10)*. Two different high speed cameras have been used for the current experimental work. A Photron Fastcam SA5 was used for the experimental work at a pressure of 5 Bar, instead of a Photron Fastcam SA-X2 that was used at 2.5 and 10 Bar. The high speed cameras were synchronized with the spark timing and the interior pressure rise recording.

2.2 Dual Fuel Mixture Preparation

For the liquid fuel, PRF95 (95%volliq iso-octane and 5%volliq n-heptane) was used. High purity (99.9%) methane was used as the gaseous fuel. The dual fuel blends consist of methane and PRF95 in three different energy ratios (25%, 50%, 75%). A blend with 25% of its energy contributing from methane as defined in Equation (1) was labelled as DF25, with 50% DF50, and for 75% DF75.

$$DF_{Ratio} = \frac{M_{CH_4} \times LHV_{CH_4}}{M_{PRF95} \times LHV_{PRF95} + M_{CH_4} \times LHV_{CH_4}} \quad (1)$$

At each initial pressure, three different equivalence ratios have been examined. The examined equivalence ratios correspond to 0.8, 1 and 1.2. For all test conditions summarised in Table 1, the air to fuel ratio was calculated using the method of chemical balance and assuming products of complete combustion. High purity technical air was used with an oxidizer concentration [O2/(O2+N2)] of 0.2 ± 0.01.

In every experimental condition, the air to fuel ratio was prepared inside the vessel using the partial pressure method. The followed methodology for deriving the partial pressures of the fuel-oxidizer is shown in Appendix A. The necessary amount of liquid and gaseous fuel was determined depending on the targeted dual fuel ratio, equivalence ratio, and the associate pressure and temperature as it is also indicated in Appendix A. Initially the vessel was heated up to the desired temperature (373 K). Whilst the heater mounted inside the vessel was turned on, the liquid fuel was injected into the combustion vessel using a multi-hole gasoline direct injector with an injection pressure of 12 MPa. The targeted fuel mass was supplied inside the combustion vessel by individual injections using pre-calibrated data. The pre-calibration process involves the determination of the mass of liquid per single injection. After the injections were completed, two minutes were given to allow for the complete evaporation of the liquid fuel. Considering the correct increase of pressure change caused by the evaporation of the liquid fuel compared to the thermodynamic ideal-gas law calculations, methane and then air fed in slowly using a fine needle valve and a pressure transducer to control the filling process. The technical air was heated by an external heater before flowing into the combustion vessel to better approximate an isothermal filling process. After the filling process was completed the interior heater was turned off, and three minutes of quiescence were given to minimize any flow

structures and/or temperature stratifications inside the vessel. The quiescence time also promotes the homogeneous mixing of fuel and air.

For each tested condition, the described experimental procedure that allowed the evaluation of the fundamental laminar flame velocity as well as burned gas Markstein length was carried out at a minimum of three times. The average values are reported as well as error bars evaluated based on standard error.

3. Post-processing Procedure

3.1 Flame Theory

A common approach of measuring burning velocity and Markstein length in a combustion vessel has been the constant pressure outwardly propagating spherical flame method *(10-16,18,19)*. The method is suitable for extrapolation of measured stretched burning velocities to their fundamental non-stretched values and the associate Markstein lengths, due to the well-defined stretch rates of an outwardly spherical flame. The constant pressure outwardly propagating spherical flame method in combination with the theory given by Strehlow and Savage *(20)* have been used by most of the studies in literature *(9,10,11,13,14)*. The theory of Strehlow and Savage derived on the assumption that the burned gas is coming to rest after crossing an infinitesimally thin flame.

In the present experimental work, the use of a cylindrical combustion vessel instead of a spherical one imposes non-symmetrical (cylindrical) confinement on the outwardly flame evolution. The non-symmetrical confinement disrupts the induced flow field from the symmetrically confined (spherical) case, causing the motion of burned gases within the burned zone even for a constant vessel pressure (*9, 21).* Significant deviations from the commonly applied flame theory can be introduced, leading to substantial errors (>15%) in the burning velocity measurements and subsequently in the derivation of laminar flame velocity.

In a cylindrical vessel, the observed propagation velocity $S_{observed}$ recorded by schlieren photography can be related to the burning velocity S_b and the flow velocity of burned gas behind the flame front (U_b, positive in the inward direction) through *(9,21)*,

$$S_{observed} = S_b - U_b \quad (2)$$

Direct application of the conventional constant pressure flame method assuming zero burned gas velocities will yield erroneous burning velocities. It has been shown that the induced error is exponentially increasing with the ratio of flame radius (R_f) to the vessel's wall (R_w) radius for $R_f > 0.3R_w$ [3]. In the current analysis, a flow-corrected burning velocity has been derived based on the model developed by M.P. Burke et al. *(9)*,

$$S_b = \frac{S_{observed}}{(1+\frac{\sigma-1}{\sigma}\bar{\omega}_r)} \quad (3)$$

where S_b is the corrected burning velocity, σ the thermal expansion factor defined as the ratio of unburned to burned gas density and $\bar{\omega}_r$ is a scaled burned gas velocity. The model accounts for the actual induced burned gas motion within the burned zone due to the non-symmetrical confinement of the flame. A detailed description of the model can be found in the publication of M.P. Burke et al. (*9*).

The method developed by Markstein (*22*), relates the stretched burning velocity with its corresponding stretch rate (a). Through relation 4, a linear extrapolation back to zero flame stretch based on the plot of of S_b versus a, can be used to derive the value of the unstretched burning velocity (S_b^0) and the associate burned gas Markstein length (L_b).

$$S_b = S_b^0 - L_b\, a \quad (4)$$

The flame stretch rate (a) can collectively describe the various influences due to flow nonuniformity, flame curvature, and flow/flame unsteadiness on the surface of an outwardly propagating spherical flame (*23)* and can be defined as,

$$a = \frac{2}{Rf} S_b \quad (5)$$

For the Markstein theory to be satisfied exactly, it requires an unwrinkled, spherical, infinitesimally thin, weakly stretched, adiabatic, quasi–steady flame with a constant expansion factor in a zero gravity, unconfined environment (*9)*. These assumptions are not satisfied in practical applications, even in well-controlled experiments.

The validity of the linear relation starts to be questionable when the Lewis number of a mixture significantly deviates from unity. As reported by Kelley and Law *(24)* a nonlinear extrapolation between stretched burning velocity and stretch rate should be used for mixtures with Lewis numbers appreciably different from unity. According to Halter et al. *(25)*, the use of a nonlinear methodology is only required when the burned gas Markstein length (L_b) reaches or surpasses the unity value (in mm). As will be illustrated in section 4.3 the maximum value of L_b measured in the current experimental study corresponds to 0.9 mm. Following the correlation derived by Halter et al. (*25)* for evaluating the relative percentage difference between linear and not linear extrapolation methodology, the maximum difference in the current experimental study corresponds to 2%. Therefore it was concluded that in the current study a linear extrapolation methodology can still be used with confidence.

Despite its limitations, the extrapolation of a spherical outwardly propagating flame to its zero stretch using the Markstein method is widely accepted and used in literature (*9-16,18)*. The Markstein theory has been used in the present study in order to allow for a comparison with the existing related literature information.

On the assumption of an infinitesimally thin flame *(20)*, the fundamental laminar flame velocity (S_u^0) can be obtained by dividing the unstretched burning velocity S_b^0 with the thermal expansion factor (σ) such as,

$$S_u^0 = \frac{1}{\sigma} S_b^0 \quad (6)$$

The required expansion factors have been computed using the model for a freely propagating flame in the Cantera software package (*26)*. The numerical model was integrated with the reduced kinetic scheme of Jerzembeck et al *(11)*.

3.2 Flame Analysis

3.2.1 Radius Definition

An in-house image processing code specifically developed for the current experimental setup was used to track the flame radius over time. The flame radius was tracked along the Y-axis as shown in Figure 2, as it is the only direction at which the adjacent walls of the vessel are symmetrical. Despite not being the same as the cold flame radius *(27)*, the schlieren image radius is commonly used in literature for flame velocity measurements (*10,11,14)*. The chronological change in flame radius determined from the gradient of a first-order least squares fit through four radii adjacent to each point under consideration *(11,12)*, allow for the calculation of the observed flame propagation velocity ($S_{observed}$). Data processed in this manner without any explicit smoothing technique, allow the most of the consistency with the raw data.

3.2.2 Upper Boundary of Analysis

The flow corrected (S_b) and uncorrected ($S_{b,unc}$) burning velocities versus stretch rate are presented in Figure 3 for a stoichiometric PRF95-air mixture at an initial pressure of 5 bar. The normalized flame radius by the vessel's wall radius (5 mm) is also presented at the top of the figure as a secondary x-axis. The burning velocity is initially increasing attributed to the effect of a decreasing stretch for a mixture of positive Markstein length. The flame appears relatively unaffected by confinement for $R_f < 0.2\ R_w$. For larger radius the non-symmetrical confinement induced the burned gas motion and the two velocities start to deviate. However, for $R_f < \approx 0.36\ R_w$, a distinct drop in burning velocity can be observed even for the corrected case. The phenomenon was consistently occurring at a flame radius of about 18 mm for all the experimental conditions and fuels. The relative pressure increase at that point was not higher than about 6%. Therefore the drastic drop in burning velocity cannot be explained by the direct effect of pressure on the reactivity of the fuel.

The radiation-induced reduction in laminar flame velocity has been quantified using the correlation proposed by Yu et al. *(28)*. The maximum reduction for the current experiments calculated to be lower than 4%. It was also concluded that radiative heat loss could not explain the drastic drop in burning velocity.

As illustrated in the schematic of Figure 1, the asymmetry in the x-axis with the presence of a wall much closer to the flame at the left side of the cylindrical vessel, is thought to promote high levels of flow field asymmetries for $R_f < \approx 0.36\ R_w$, that distort the flame from its spherical shape.

To help the reader visualize the mentioned phenomenon, a symbolic illustration is presented in Figure 4. The figure presents indicative flame surface contours as experienced during the current experimental work (solid lines), as compared to contours that would correspond to an unconfined flame evolution (dotted lines). At the early stages (i.e a,b), the burned gas is relatively motionless and the flame shape remains similar to that of the unconfined case. However, in contrast to the unconfined case, as the flame develops (i.e c-d-e), the burned gas deviates from its motionless state causing a non-similar flame propagation velocity along the X as compared to the Y direction. For large flame radius (i.e d-e), high levels of flow field asymmetries significantly distort the flame from its spherical shape.

As suggested by M.P.Burke et al. *(9)*, the accuracy of the model is expected to be questionable in a strongly disrupted flow field. It was therefore necessary to limit the analysis of flames up to a maximum radius of 18 mm ($0.36\ R_w$) to avoid high levels of induced flow field asymmetries that degrades the accuracy of the flow-correction model.

3.2.3 Lower Boundary of Analysis

The early stage of flame evolution is influenced by ignition transients that affect the measured value of burning velocity. The effects are more prominent for mixtures of high Lewis number (*29)*. In the current experimental conditions, PRF95 is having the highest Lewis number. As suggested by Bradley et al. *(12)*, the sharp fall in burning velocity with stretch rate indicates that in this regime a fully developed flame is not yet established. Following the previous comments, data have been excluded for radii below 7 mm at 2.5 Bar, 6 mm at 5 Bar, and 5 mm at 10 Bar. The resulted values are consistent with literature, as different researches (11,*12,17,30)* suggest that ignition transients diminish at flame radii between 5 -10 mm. Consequently, having defined the upper and lower boundaries, the smallest range of analysis (11mm) corresponds to a pressure of 2.5 bar. Within this range there is a minimum of 21 data points available for the extrapolation technique to be applied. Similar amount of data points as the minimum amount in the current experimental work have been successfully used by Kelley and Law *(24)* for their extrapolations of S_b to zero stretch.

3.2.4 Extrapolation Technique

The unstretched burning velocity (S_b^0) and the corresponding Markstein length (L_b), can be determined using a linear extrapolation through the largest possible range of radii where there is no spark influence and where the curve of S_b versus stretch rate is reasonably linear (*12)*. Historically, the choice of data range has been somewhat arbitrary. Different researchers made different choices without giving quantitative justification *(21)*. In an effort to derive the values of S_b^0 and L_b with a consisted approach a sensitivity analysis has been performed through the selected reasonably linear range of radii.

The overall methodology is depicted in Figure 5, whereas the axes have been magnified to point out the oscillatory trend of S_b purely for presentation purposes. The observed oscillations of S_b are induced by the unavoidable acoustic disturbances inside the vessel *(11,12)*. The lower boundary of the sensitivity analysis is defined as the first point of the selected reasonably linear range. An extrapolated line is fitted starting from the lower boundary and moving with increments of 0.5 mm in radius towards the upper boundary. The upper boundary is defined as the point at which L_b changes sign compared to its initial sign at the lower boundary. Each extrapolated line within the range of sensitivity analysis is giving a value of S_b at zero stretch (S_b^0). The selected S_b^0 is defined as the average within one standard deviation of all the resulted values. The intersection of the extrapolated line giving the closest value to the derived S_b^0 (dotted red), is used to define the value of L_b.

For each investigated pressure and equivalence ratio, five different fuels have been tested with a minimum of three repeats per fuel. A sensitivity analysis has been performed for each investigated point to determine the value of S_b^0. At each pressure, the average standard deviation ($\bar{\sigma}$) and average S_b^0 ($\overline{S_b^0}$) of all tested fuels is calculated at each equivalence ratio. The induced uncertainty on S_b^0 due to the extrapolation technique presented in Figure 6 is defined as,

$$\Delta S_b^0 = \left(1 - \frac{\overline{S_b^0} - \bar{\sigma}}{\overline{S_b^0}}\right) * 100 \quad (7)$$

The trend of the induced uncertainty due to the extrapolation procedure appears to increase with the decrease of pressure attributed to a reduced amount of available data points for extrapolation within the selected linear range.

4. Results – Discussion

4.1 Flame Evolution and Morphology

The evolution of a stable flame is mainly governed by the laminar flame velocity (S_u^0) of the fuel-oxidizer mixture, and the sensitivity of that flame to stretch characterised by the Markstein length (L_b).

At a pressure of 5 Bar, the mean flame evolutions selected among the different repeats of each fuel, at each tested equivalence ratio, are presented in the left plots of Figure 7.The flame evolutions, defined as flame radii over time, are presented on a logarithmic scale up to a radius of 15mm along with the time elapsed from the point of spark. At respective time steps up to 6.7 ms, the percentage difference of the flame's radius of each fuel in comparison to that of the pure liquid fuel (PRF95) has been calculated and shown in the right plots of Figure 7. A Dual Fuel (DF) ratio of 0% corresponds to the pure liquid fuel (PRF95) whereas 100% corresponds to the gaseous fuel (CH_4).

At lean conditions ($\Phi = 0.8$), It has been observed that at 0.8 ms after spark, the flame radius is increased with the addition of methane to PRF95 in a dual fuel blend. There is 41% difference between the radius of methane in comparison to that of

PRF95. The characteristic *S* shape corresponding to the flame evolution of PRF95 is due to the phenomenon of flame reverse. The phenomenon is found to be most prominent in mixtures of relatively high Lewis numbers *(29)*. Flame reverse phenomena are observed for PRF95 and to a much lower extend DF25 only at lean conditions. At 3.3 ms after spark, the flame radius of DF50 is larger than double the radius of PRF95. From 3.3 ms onwards, the flame evolution of the DF50 and DF25 is similar. The flame evolution of DF75 and methane are diverging from the one of DF50 whereas that of PRF95 is converging towards DF50 up to 10 ms, and then gradually starts to diverge. As far as flame evolution is concerned, similar phenomena is observed at 2.5 Bar, whereas at 10 Bar all DFs including methane are having a faster evolution than PRF95 at the early stages of combustion and slower in the developed flame regime.

At lean conditions, the effect of dual fuelling in the flame evolution is of particular practical importance. To allow for the visualization of flame evolution, chronological schlieren images of three selected fuels CH_4, DF50 and PRF95 are presented in Figure 8. There are no signs of flame wrinkling or any indication of cellular structures up to the maximum radius of analysis. The shape of the flames looks smooth independently of the fuel. Although particular attention has been applied on minimizing the effect of the electrodes on the morphology of the flame by adjusting their diameter and inter distance, the effect could not be totally eliminated. Similar visual effects owning to the electrode and flame interactions have been reported in other experimental studies in literature *(11,18,31)*.As far as flame morphology at lean conditions is concerned, flames at a pressure of 2.5 Bar and 10 Bar shown consisted behavior as in the 5 Bar case.

At stoichiometric conditions ($\Phi = 1$), the qualitative response of flame evolution to the DF ratio at 0.8 ms after spark, is the same as in the lean conditions. From 1.7 ms onwards, the flame evolution of the DF50 mixture forms a medium between the tested fuels. The flame evolution of PRF95 and DF25 are converging towards DF50 in contrast to DF75 and methane that are diverging. Similar trends in flame evolution could be observed at a pressure of 2.5 Bar. At a pressure of 10 Bar, the flame evolution of the DF75 mixture resulted to be considerably faster compared to the rest of the fuels. The response was consistent for all of its repeats.

The morphology of the DF flames at a randomly selected radius of about 10 mm is illustrated in Figure 9. The wrinkling on the flame surface is increased with the DF ratio, although cellular structures could not be observed up to the maximum radius of analysis. This is in contrast to the observations of flame stability at 2.5 and 5 Bar where flames are relatively free of wrinkles.

As proposed by Rozenchan et al. *(16)* and supported by L.Qiao et al. *(32)* at the absence of cell cracking to smaller scales (cellularity) the linear relationship between burning velocity and stretch still holds. The faster flame evolution of DF75 at a pressure of 10 Bar is thought to be caused by phenomena of flame instability. The effects of developed instability on the flame evolution are out of the scope of this study.

At rich conditions (Φ = 1.2), the response of the flame evolution to the DF ratio is totally different compared to the lean conditions. At 0.8 ms after spark, the flame radius is decreased with the addition of methane to PRF95 in a dual fuel blend. All DFs have a slower flame evolution compared to PRF95. As the flame develops, the flame evolution of DF50 and DF75 becomes slower even compared to that of methane. The trend in flame evolution with respect to the DF ratio is similar at 2.5 Bar. However, at a pressure of 10 Bar cellular structures have been observed for all DFs altering the flame evolution and leading to faster flames even compared to those of PRF95. Rich flames at a pressure of 10 Bar have been excluded from further analysis.

With the addition of methane to PRF95 is evident that flame evolution is altered in all equivalence ratios. In the present study, the evaluation of laminar flame velocity and Markstein length will enhance the understanding on the mechanism behind the response of flame evolution with the DF ratio. For all tested conditions, the effects of methane addition to PRF95 on both fundamental combustion parameters will be quantified.

4.2 Stretch Effects

Using the same data as for the plots of flame evolution in the previous section, the stretched burning velocity versus flame stretch is plotted in Figure 10 for CH_4, DF50 and PRF95 at three different equivalence ratios, and a pressure of 5Bar. The presented burning velocitys correspond to flame radii between 6 to 15 mm. The influence of flame stretch on the burning velocity is characterised by the value of burned gas Markstein length (L_b). The fitted lines resulted from the extrapolation technique, and used for calculating L_b, are also presented.

At lean conditions ($\Phi = 0.8$), as flame stretch increases, the burning velocity of PRF95 is decreased attributed to a positive L_b whereas that of methane is increased due to the negative L_b. The burning velocity of DF50 remains relatively unaffected by flame stretching. For the whole range of flame stretch, DF50 has a faster burning velocity than PRF95. The difference is gradually increasing with flame stretch. Following the extrapolated lines, the burning velocity of methane becomes faster than that of PRF95 at a flame stretch of about 600 1/s. At stoichiometric conditions ($\Phi = 1$), the burning velocity of all fuels is decreased with the flame stretch. However, as the DF ratio is increased, the sensitivity of the burning velocity to the flame stretch is reduced. As flame stretch increases, the burning velocity of methane and DF50 converges and eventually becomes faster as compared to the velocity of PRF95. The burning velocity of the DF50 blend becomes faster than that of PRF95 at a flame stretch of about 300 1/s. At rich conditions ($\Phi = 1.2$), methane's flame is having the largest sensitivity to stretch followed by PRF95 and DF50. All fuels are having a positive L_b although DF50 has a value close to zero. For the whole range of flame stretch the burning velocity of PRF95 is higher than the velocity of methane and DF50. It is evident from Figure 10 that the response of burning velocity to the flame stretch characterised by L_b is depended both on the equivalence ratio and on the particular fuel under consideration.

4.3 Markstein Length

The response of L_b with respect to the DF ratio as well as pressure is depicted in Figure 11, for each tested equivalence ratio. At each investigated point, error bars are evaluated based on the standard error of all the repeated tests. The uncertainty of the extrapolation procedure and the repeatability of the tests at each investigated point are contributing to the extent of the error bars. Available literature data are also presented in Figure 11 for the base fuels. It appears that there is no prior work reporting values of L_b for different ratios of methane addition to PRF95 at elevated pressures. For presentation purposes, some of the literature data are slightly shifted on the x-axis. At each test pressure, the data are correlated with a suitable fit (solid lines) aiming to present the overall trend of L_b versus DF ratio. A quadratic relationship has been applied for lean and rich conditions and a linear relationship for stoichiometry. The coefficients of the resulted fits are presented in Table 2.

Methane being the lightest hydrocarbon among the tested fuels is found to have the lowest L_b at lean and stoichiometric conditions, and the highest at rich conditions. In contrast, PRF95 being the heaviest hydrocarbon, shown opposite response to that of methane. Similar phenomena have been reported in literature (*15,18)*. At lean conditions, with the increase of DF

ratio the values of L_b are reduced following a quadratic relationship in the form of $a\ DF_{ratio}^{\ 2} + b\ DF_{ratio} + c$. At a pressure of 2.5 Bar, the values of L_b for all DFs are converging to that of methane. As pressure is increased, the reduction in L_b with the DF ratio gradually becomes more linear. At stoichiometric conditions, with methane addition to PRF95 there is a linear decrease in L_b for all tested pressures. Following the fitted lines of the form $a\ DF_{ratio} + b$, with a 25% increase in DF ratio, the value of L_b is reduced by 16%, 20%, 28% at a pressure of 2.5, 5, and 10 Bar respectively. At rich conditions, the response of L_b with DF ratio is contrary to the stoichiometric and lean conditions, with DF75 and methane being more sensitive to flame stretch than PRF95 at a pressure of 2.5 Bar. At 5 Bar all DFs found to have lower values of L_b as compared to PRF95 and to larger extend methane.

For the three tested equivalence ratios, the response of L_b is not only affected by a change in fuel but is also affected by a change in pressure. As pressure increases the value of L_b is reduced for all fuels as can be clearly observed in Figure 11. For a given fuel-air mixture, the absolute value of L_b decreases with an increase in pressure attributed to the reduction of flame thickness *(33)*. Due to the reduced flame thickness, the stretch induced on the flame by its curvature and flow straining is reduced, and therefore the flame become less sensitive to stretch manifested by a lower value of L_b.

Available literature data are also presented in Figure 11. Bradley et al. *(12)* reported values of L_b for an iso-octane-air mixture at different pressures, temperatures and equivalence ratios. Appropriate values from that study are illustrated in Figure 11 (+ markers) for a comparison to the values of PRF95 resulted from the current study. Mandilas et al. *(18)* reported values of L_b for both methane and iso-octane air mixtures at 5Bar and 360K. Values from this study are reported with rectangles. Also for methane, the reported values of L_b from the experimental studies of Rozenchan et al. *(16)* (star markers), and Gu et al. *(15)* (x markers), are presented. Considering the reported discrepancies of the measured Markstein lengths by different researchers *(34)* that can be even larger than 300%, it can be concluded that the reported values of L_b from the current experimental work are in satisfactory quantitative and qualitative agreement with the selected values from literature.

4.3.1 Mass Diffusivity and Markstein Length

The response of L_b with the equivalence ratio for all tested fuels at a pressure of 5 Bar is illustrated in Figure12. The Markstein length is depended on thermodynamics and transport properties of the combustible mixture *(35-37)*. In particular, L_b is found to be mainly governed by the thermo-diffusive properties, the so-called Lewis number effect *(36-39)*. The Lewis number is defined as the ratio of thermal to mass diffusivity of the combustible mixture. In general, for a mixture of Lewis number higher than unity, L_b is expected to be positive and for Lewis number lower than unity negative. As stated by Law and Sung *(37)* this argument still holds even if only the relative mass diffusivities of the fuel and oxidizer species are considered. For a sufficiently off stoichiometric mixture where its mass diffusivity (D) can be approximated as that of the deficient reactant (fuel for lean and oxidizer for rich conditions); If the diffusivity of the fuel is higher/lower than the diffusivity of the oxidizer, L_b is expected to be negative/positive. As proposed by Law and Sung *(37)* based on molecular

weight considerations, as the fuel molecule becomes lighter, the diffusivity of the fuel relative to air increases. Following the mentioned reasoning, the diffusivity of the fuel relative to air increases with the DF ratio.

Although an equivalence ratio of 0.8 does not reflect a sufficiently off-stoichiometric mixture, the diffusivity of the fuel can be reasonably assumed representative to that of the mixture. As can be observed from Figure 12, L_b is inversely scaled with the mass diffusivity of the fuels. The mass diffusivity of the fuel is increased with DF ratio leading to a reduction in L_b. It has been found that the relative values of L_b for all DFs converge to that of methane at lean conditions. The mass diffusivity of the base fuels in a DF mixture is considerable different (for example, $D_{CH4} = 21.9$ mm^2/s and $D_{iC8H18} = 6.6$ mm^2/s *(35)*). Considering the difference of the mass diffusivity of the base fuels as well as their mole fractions in the different DFs shown in Table 1, the effective diffusivity of the DF mixtures is thought to be proportionally biased towards that of methane. Similar phenomena have been discussed for a mixture of methane and hydrogen in the study of Dinkelacker et al. *(39)*.

For stoichiometric conditions, the diffusivity of the mixture is expected to depend on both the diffusivity of air and fuel. In contrast to PRF95, for methane and all DFs the value of L_b at stoichiometric conditions is increased compared to the lean conditions. As the DF ratio is reduced the increase in L_b is lower. This response supports our thoughts that the effective diffusivity of a DF mixture is proportionally biased towards that of methane. At rich conditions, the deficient reactant is air and all fuel air mixtures are expecting to converge to a single diffusivity, that of air. As can be observed from Figure 12, the values of L_b seem to converge for all investigated fuel air mixtures.

It has to be pointed out that at lean conditions and a pressure of 2.5 Bar although the reduction of L_b with the DF ratio can be qualitatively explained by the proposed theory, methane does not show a negative value of L_b. It can be concluded that the effective mass diffusivity is definitely a major contributor to the response of L_b with equivalence ratio for the different DFs, however it is not adequate for a quantified explanation.

4.4 Laminar Flame Velocity

Following the evaluation of L_b, values of the laminar flame velocity (S_u^0) for all investigated conditions are presented in Figure 13 with available literature data. Similar to the analysis of L_b, suitable fits (solid lines) are also presented with their coefficients reported in Table 3. At stoichiometric conditions and a pressure of 10 Bar, the value of S_u^0 for the DF75 blend is considerably higher compared to the rest of the fuels. As discussed in section 4.1, DF75 is thought to be affected by phenomena of flame instability therefore its velocity is not taken into consideration for the linear fit correlation.

Methane resulted to have a lower S_u^0 than PRF95 at all investigated conditions. Interestingly, at lean conditions it has been found that by blending methane with PRF95 the resulted S_u^0 of all DFs is larger even compared to that of PRF95 at a pressure of 5 Bar and to less extent 2.5 Bar. The only exemption corresponds to the DF75 blend at 2.5 Bar. At a pressure of 10 Bar, with the increase of the DF ratio the value of S_u^0 is reduced. However the velocity of all DFs converges to that of PRF95. At stoichiometric conditions, with the increase of DF ratio there is a linear decrease in S_u^0 for all tested pressures.

Following the fitted lines, with a 25% increase in DF ratio, the value of S_u^0 is reduced by 2%, 4%, 5% at a pressure of 2.5, 5, and 10 Bar respectively. At rich conditions the response of S_u^0 with DF ratio is contrary to that at lean conditions. All DFs resulted to have a lower S_u^0 even compared to that of methane.

The recent study of Baloo et al. (*19)*, conducted at atmospheric pressure, reported similar findings on the response of S_u^0 with the DF ratio. The chemical paths leading to the initiation and/or recombination reactions during the combustion of a DF blend can explain the response of S_u^0 with the DF ratio. However, as stated by Baloo et al. [13] and supported by the authors, detailed chemical kinetics of the blend fuel that will develop the understanding on the response of S_u^0 with the DF ratio are currently unavailable.

The adverse effect of pressure on S_u^0 is clearly shown in Figure 13. As pressure increases the value of S_u^0 is decreased for all investigated conditions. According to Galmiche et al. *(30)* at high pressures the recombination reaction $H+ O_2 + M \rightarrow HO_2 + M$ reduces the H atom concentration and thus competes with the initiation reaction $H + O_2 \rightarrow O + OH$ producing free radicals O and OH. This process tends to reduce the overall oxidation rate and to inhibit the combustion reaction. This finding is also supported by C.K. Law *(23)*, although he is suggested that the increase of the unburned gas density with pressure is the main contributor for the reduction in flame velocity.

Available literature data are also included in Figure13. For methane, data are taken from the work of Gu et al. (x marks) *(15)* and Mandilas et al. (rectangles) *(18)*. For PRF95, data are taken from the work of Bradley et all (+ marks) (*12)*, Jerzembeck et al. (triangles) (*11)*, Beeckmann et al. (circles) *(14)* and Mandilias et al. (rectangles) *(18)*. It appears that there is no prior literature study reporting values of S_u^0 for methane-PRF95 dual fuel blends at elevated pressures. At a pressure of 2.5 Bar, the experimental values of S_u^0 for PRF95 obtained in this work are on average 22% higher compared to those reported in literature. For the rest of the experimental tests, there is a maximum deviation of 12% between the values of S_u^0 obtained in this work as compared to the ones reported in literature at the same temperature.

5. Dual Fuelling Synergies

With the evaluation of both fundamental combustion parameters L_b and S_u^0, the mechanism of the flame evolution as discussed in section 4.1 can now be explained. For convenience, due to the linear fitted correlations, the discussion will be related to the stoichiometric mixtures although is applicable to both lean and rich conditions. At a pressure of 5 Bar, with a 25% increase in the DF ratio, the values of S_u^0 and L_b are reduced by 4% and 20% respectively. As already discussed, at the early stages of combustion the flame radius is increased with DF ratio. It is clear that the mechanism behind this phenomenon is attributed to the decrease of L_b as the dual fuel ratio is increased. As the flame develops and flame radius is increasing, stretch rate is reduced. This implies that the effect of L_b on the flame velocity is decaying. Therefore S_u^0 will start

to dominate the flame evolution. As a result, an increase in the DF ratio will delay the flame evolution. Indeed at stoichiometric conditions, the flame evolution of PRF95 becomes faster and that of methane slower as the combustion process progress. From the scope of Markstein Length, methane seems a suitable fuel for real combustion applications where from the scope of laminar flame velocity PRF95 has a distinct advantage over methane.

At lean conditions, it has been found that there is a distinct synergy in blending methane with PRF95 as the advantages of the light and heavy hydrocarbon fuels are combined to form a suitable fuel blend for future lean burn energy efficient combustion applications. For a DF blend, the Markstein length that dominates the early stages of combustion has been found to converge to that of methane, whereas the laminar flame velocity that governs the developed flame propagation regime is even higher than that of PRF95. The synergy for Methane-PRF95 dual fuelling arise from the advantageous combination of these two fundamental combustion parameters L_b and S_u^0 that allows for the flame evolution of DF50 blend to be up to 1.2 times faster compared to that of PRF95 at lean conditions.

6. Conclusions

The effects of methane addition to PRF95 on the fundamental combustion parameters, laminar flame velocity (S_u^0) and Markstein length (L_b), were experimentally investigated in a cylindrical combustion vessel at equivalence ratios of 0.8,1,1.2 , initial pressures of 2.5, 5, 10 Bar and a constant temperature of 373 K. Methane was added to PRF95 in three different energy ratios 25%, 50% and 75%. Spherically expanding flames were used to derive the flow corrected burning velocitys, from which the corresponding L_b and S_u^0 were obtained.

At lean conditions, It has been found that the sensitivity of the flame to stretch for all DFs, characterised by L_b, is biased towards that of methane being the least sensitive. The effect decays as pressure increases. In contrast, at rich conditions the values of L_b for all DFs were lower than methane and comparable to those of PRF95. At stoichiometric conditions, with a 25% increase in the DF ratio, the value of L_b is reduced by 16% , 20% , 28% at a pressure of 2.5 , 5 and 10 Bar respectively. As pressure increases, L_b is reduced for all fuels. A satisfactory qualitative and quantitate agreement with the appropriate values from literature was obtained for the base fuels.

As far as S_u^0 is concerned, at lean conditions all DFs are faster than PRF95 at 2.5 and 5 Bar. At 10 Bar the values of S_u^0 for all DFs is comparable to that of PRF95. In contrary, at rich conditions all DFs are slower even compared to methane. At stoichiometric conditions, with a 25% increase in the DF ratio the value of S_u^0 is reduced by 2% , 4% and 5% at pressure of 2.5 , 5 and 10 Bar respectively. As pressure increases, S_u^0 is reduced for all fuels. The measured values of PRF95 at 2.5 Bar are on average 22% higher compared to literature. Excluding these values, there is a maximum deviation of 12% between the values of S_u^0 obtained in this work and those reported in literature.

At lean conditions, it has been found that the values of L_b for all DFs can be similar to those of methane with values of S_u^0 being even higher than those of PRF95. These findings indicate a distinct synergy for the utilization of dual fuelling in energy efficient lean burn combustion applications.

Appendix A

The targeted DF ratio ($\boldsymbol{DF_{Ratio}}$), equivalence ratio ($\boldsymbol{\Phi}$), temperature ($\boldsymbol{T}$) and pressure ($\boldsymbol{P}$) in a particular test condition have to be given as inputs for the calculation of the partial pressures of the fuel-oxidizer, and their masses in the combustion vessel.

Fuel-air mixtures can be considered as,

$$X_{CH_4} + \left(1 - X_{CH_4}\right)\left(x_{C_8H_{18}} C_8H_{18} + x_{C_7H_{16}} C_7H_{16}\right) + Z\ (O_2 + 4\ N_2) \quad \text{(A.1)}$$

Where X_{CH_4} is the methane mole fraction in the blended fuel, and $x_{C_8H_{18}}$, $x_{C_7H_{16}}$ is the iso-octane and n-heptane mole fraction in the base PRF95 fuel corresponds to 0.943 and 0.057 respectively. The number of oxygen moles per mole of the blended fuel is indicated with the letter Z.

Considering the lower heating value of methane $\left(LHV_{CH_4} = 50\ kJ\ kg^{-1}\right)$ and PRF95 ($LHV_{PRF95} = 44.66\ \ kJ\ kg^{-1}$), and given the energy fraction of methane $\left(E_{CH_4}\right)$, and PRF95 (E_{PRF95}) in the DF mixture, the partial pressures of the base fuels and the partial pressure of air can be evaluated following the analysis below,

$$DF_{Ratio} = E_{CH_4} \quad \text{(A.2)}$$

$$E_{PRF95} = 1 - E_{CH_4} \quad \text{(A.3)}$$

$$E_{DF} = E_{CH_4} LHV_{CH_4} + E_{PRF95}\ LHV_{PRF95} \quad \text{(A.4)}$$

Where E_{DF} is the total fuel energy in the DF blend. The mass fraction of methane $\left(Y_{CH_4}\right)$ and PRF95 (Y_{PRF95}) in the DF blend can be defined as,

$$Y_{CH_4} = E_{CH_4}\ E_{DF}\ /\ LHV_{CH_4} \quad \text{(A.5)}$$

$$Y_{PRF95} = 1 - Y_{CH_4} \quad \text{(A.6)}$$

The mean molecular mass ($\bar{W}$) of the blended fuel is calculated through,

$$\bar{W}_{Fuel} = \frac{1}{\frac{Y_{CH_4}}{W_{CH_4}} + \frac{Y_{PRF95}}{W_{PRF95}}} \quad \text{(A.7)}$$

Where W_{CH_4}, W_{PRF95} are the molecular masses of methane and PRF95 respectively. The molecular mass of PRF95 (W_{PRF95}) is given by,

$$W_{PRF95} = x_{C_8H_{18}} W_{C_8H_{18}} + x_{C_7H_{16}} W_{C_7H_{16}} \quad \text{(A.8)}$$

The mole fraction of methane (X_{CH_4}) and PRF95 (X_{PRF95}) is calculated as,

$$X_{CH_4} = Y_{CH_4} \overline{W}_{Fuel} / W_{CH_4} \quad \text{(A.9)}$$

$$X_{PRF95} = 1 - X_{CH_4} \quad \text{(A.10)}$$

The gravimetric Air to Fuel Ratio (AFR) of the DF-air mixture assuming products of complete combustion and an oxidizer concentration [O2/(O2+N2)] of 0.2 is defined as,

$$AFR = [(1/\Phi)(a + b/4)5W_{Air}] / \overline{W}_{Fuel} \quad \text{(A.11)}$$

Where a and b is the carbon and hydrogen atoms in the DF blend,

$$a = 7.94X_{PRF95} + X_{CH_4} \quad \text{(A.12)}$$

$$b = 17.89X_{PRF95} + 4X_{CH_4} \quad \text{(A.13)}$$

The mass fraction of the fuel (Y_{Fuel}) and air (Y_{Air}) in the blended fuel- air mixture is calculated as,

$$Y_{Fuel} = 1/(AFR + 1) \quad \text{(A.14)}$$

$$Y_{Air} = AFR/(AFR + 1) \quad \text{(A.15)}$$

The mole fraction of the fuel (X_{Fuel}) and air (X_{Air}) in the blended fuel and air mixture is obtained as,

$$X_{Fuel} = Y_{Fuel} \overline{W}_{Mix} / \overline{W}_{Fuel} \quad \text{(A.16)}$$

$$X_{Air} = Y_{Air} \overline{W}_{Mix} / \overline{W}_{Air} \quad \text{(A.17)}$$

Where $\overline{W}_{Air}$ the molecular mass of pure air, $\overline{W}_{Mix}$ is the molecular mass of blended fuel-air mixture,

$$\overline{W}_{Air} = 0.2W_{O_2} + 0.8W_{N_2} \quad \text{(A.18)}$$

$$\overline{W}_{Mix} = \frac{1}{\frac{Y_{Fuel}}{\overline{W}_{Fuel}} + \frac{Y_{Air}}{\overline{W}_{Air}}} \quad \text{(A.19)}$$

The mole fraction of the base fuels in the blended fuel air mixture is calculated as,

$$X_{PRF95_{Mix}} = X_{PRF95} X_{Fuel} \quad \text{(A.20)}$$

$$X_{CH_{4Mix}} = X_{CH_4} X_{Fuel} \quad \text{(A.21)}$$

Finally the partial pressure of the base fuels and the partial pressure of air are given by,

$$P_{PRF95} = X_{PRF95_{Mix}} P \quad \text{(A.22)}$$

$$P_{CH_4} = X_{CH_{4_{Mix}}} P \quad \text{(A.23)}$$

$$P_{Air} = X_{Air} P \quad \text{(A.24)}$$

Using the ideal gas law, the total mass (M_{Mix}) in the combustion vessel can be described as,

$$M_{Mix} = \bar{W}_{Mix} P V_{CVCV} / RT \quad \text{(A.25)}$$

The mass of base fuels and the mass of air in the combustion vessel is given by,

$$M_{PRF95} = M_{Mix} Y_{Fuel} Y_{PRF95} \quad \text{(A.26)}$$

$$M_{CH_4} = M_{Mix} Y_{Fuel} Y_{CH_4} \quad \text{(A.27)}$$

$$M_{Air} = M_{Mix} Y_{Air} \quad \text{(A.28)}$$

References

(1) A. Boretti, P. Lappas, B. Zhang, and S. Mazlan, CNG Fuelling Strategies for Commercial Vehicles Engines – A Literture Review, SAE Technical Paper (2013), paper 2013-01-2812.

(2) B. Douailler, F. Ravet, V. Delpech, and D. Soleri, B. Reveille, R. Kumar, Direct Injection of CNG on High Compression Ratio Spark Ignition Engine: Numerical and Experimental Investigation, SAE Technical Paper (2011), paper 2011-01-0923.

(3) Z. Huang, Y. Zhang, K. Zeng, B. Liu, Q. Wang, D. Jiang, Measurements of laminar burning velocities for natural gas-hydrogen-air mixtures, Combust. Flame 146 (2006) 302-311.

(4) E.Hu, Z. Huang, J. He, C. Jin, J. Zheng, Experimental and numerical study on laminar burning characteristics of premixed methane-hydrogen-air flames. Int. J. Hydrogen Energy 34 (2009) 4876-4888.

(5) E. Hu, Z. Huang, J. He, J. Zheng, H. Miao, Measurements of laminar burning velocities and onset of cellular instabilities of methane-hydrogen-air flames at elevated pressures and temperatures, Int. J. Hydrogen Energy 34 (2009) 5574-5584.

(6) S. Petrakides, D. Gao, R. Chen, D. Butcher, W. Haiqiao, Experimental Study on the Burning Rate of Methane and PRF95 Dual Fuels, SAE Int. J. Engines 9 (2016), paper 2016-01-0804.

(7) S. Di Iorio, P. Sementa, and B. Vaglieco, Experimental Investigation of a Methane-Gasoline Dual-Fuel Combustion in a Small Displacement Optical Engine, SAE Technical Paper (2013), paper 2013-24-0046.

(8) S. Di Iorio, P. Sementa, B. Vaglieco, and F. Catapano, An experimental investigation on combustion and engine performance and emissions of a methane-gasoline dual-fuel optical engine, SAE Technical Paper (2014), paper 2014-01-1329.

(9) M.P. Burke, Z. Chen, Y.Ju, F.L. Dryer, Effect of cylindrical confinement on the determination of laminar flame speeds using outwardly propagating flames, Combust. Flame 156 (2009) 771-779.

(10) G. Tian, R. Daniel, H. Li, H. Xu, S. Shuai, P. Richards, Laminar Burning Velocities of 2,5-Dimethylfuran Compared with Ethanol and Gasoline, Energy Fuels 24 (2010) 3898-3905.

(11) S. Jerzembeck, N. Peters, P.P. Desjardins, H. Pitsch, Laminar burning velocities at high pressure for primary reference fuels and gasoline: Experimental and numerical investigation, Combust. Flame 156 (2009) 292-301.

(12) D. Bradley , R.A. Hicks, M. Lawes, C.G.W. Sheppard, E. Wolley, The Measurement of Laminar Burning Velocities and Markstein Numbers for Iso-octane–Air and Iso-octane–n-Heptane–Air Mixtures at Elevated Temperatures and Pressures in an Explosion Bomb, Combust Flame 115 (1998) 126-144.

(13) O. Mannaa, M.S. Mansour , W.L. Roberts, S.H. Chung, Laminar burning velocities at elevated pressures for gasoline and gasoline surrogates associated with RON, Combust. Flame 162 (2015) 2311-2321.

(14) J.Beeckmann, O.Rohl, N.Peters, Numerical and Experimental Investigation of Laminar Burning Velocities of iso-Octane, Ethanol and n-Butanol, SAE Technical Paper (2009), paper 2009-01-2784.

(15) X.J. Gu, J.M. Lawes, R. Wooley, Laminar burning velocity and Markstein lengths of methane–air mixtures, Combust.Flame 121 (2000) 41-58.

(16) G. Rozenchan, D.L. Zhu, C.K. Law, S.D. Tse, Outward propagation, burning velocities, and chemical effects of methane flames up to 60 atm , Proc. Combust. Inst. 29 (2002) 1461-1469.

(17) M.I. Hassan, K.T. Aung, G.M. Faeth, Measured and predicted properties of laminar premixed methane/air flames at various pressures, Combust. Flame 115 (1998) 539-550.

(18) C. Mandilias, M.P. Ormsby, C.G.W. Sheppard, R. Wooley, Effects of hydrogen addition on laminar and turbulent premixed methane and iso-octane-air flames, Proc. Combust. Inst. 31 (2007) 1443-1450

(19) M. Ballo, B.M. Dariani, M. Akhlaghi, I. Chitsaz, Effect of iso-octane/methane blend on laminar burning velocity and flame instability, Fuel 144 (2015) 264-273.

(20) R.A. Strehlow, L.D. Savage, The Concept of Flame Stretch, Combust. Flame 31 (1978) 209-211.

(21) Z. Chen, M.P. Burke, Y. Ju, Effects of compression and stretch on the determination of laminar flame speeds using propagating spherical flames, Combust. Theory and Modelling 13:2 (2009) 343-364.

(22) G.H. Markstein, Non-Steady Flame Propagation, Pergamon , New York, 1964, p22.

(23) C.K. Law, Combustion Physics, Cambridge, New York, 2006, p 405.

(24) A.P.Kelley, C.K.Law, Nonlinear effects in the extraction of laminar flame speeds from expanding spherical flames, Combust. Flame 156 (2009) 1844-1851.

(25) F.Halter, T.Tahtouch, C.Mounaim-Rousselle, Nonlinear effects of stretch on the flame front propagation, Combust. Flame 157 (2010) 1825-1832.

(26) D. Goodwin, N. Malaya, H. Moffat, R. Speth, Cantera: An object-oriented software toolkit for chemical kinetics, thermodynamics, and transport processes. Version 2.2 available at https://code.google.com/p/cantera/, [Accessed 10 September 2015].

(27) D. Bradley, P.H. Gaskell , X.J. Gu, Burning velocities, markstein lengths, and flame quenching for spherical methane-air flames: A computational study, Combust. Flame 104 (1996) 176-198.

(28) H. Yu, W. Han, J. Santner, X. Gou, C. H. Sohn, Y. Ju, Z. Chen, Radiation-induced uncertainty in laminar flame speed measured from propagating spherical flames, Combust. Flame 161 (2014) 2815-2824.

(29) Z. Chen, M.P. Burke, Y. Ju, Effects of Lewis number and ignition energy on the determination of laminar flame speed using propagating spherical flames, Proc. Combust. Inst. 32 (2009) 1253-1260.

(30) B. Galmiche, F. Halter, F. Foucher, Effects of high pressure, high temperature and dilution on laminar burning velocities and Markstein lengths of iso-octane/air mixtures, Combust. Flame 159 (2012) 3286-3299.

(31) M.C. Krejci, O.Mathieu, A.J. Vissotski, S.Ravi, T.G. Sikes, E.L. Petersen, A.Kermones, W. Metcalfe, H.J.Curran, Laminar Flame Speed and Ignition Delay Time Data for the Kinetic Modeling of Hydrogen and Syngas Fuel Blends, ASME J. Eng. Gas Turbines Power, 135, (2013), 021503-1.

(32) L. Qiao, C.H. Kim, G.M. Faeth, Suppression effects of diluents on laminar premixed hydrogen/oxygen/nitrogen flames, Combust. Flame, 143, (2005), 79-96.

(33) C.J. Sun, C.J. Sung, L. He, C.K. Law, Dynamics of weakly stretched flames: quantitative description and extraction of global flame parameters, Combust. Flame 118 (1999) 108-128.

(34) Z. Chen, Effects of radiation and compression on propagating spherical flames of methane/air mixtures near the lean flammability limit, Combust. Flame 157 (2010) 2267-2276.

(35) J.K. Bechtold, M. Matalon, The dependence of the Markstein length on stoichiometry, Combust. Flame, 127, (2001), 1906-1913.

(36) U.C. Muller, M. Bollig, N. Peters, Approximations for burning velocities and markstein numbers for lean hydrocarbon and methanol flames, Combust. Flame 108 (1997) 349-356.

(37) C.K. Law, C.J. Sung, Structure, aerodynamics, and geometry of premixed flamelets, Progress Energy Combust. Sci. 26 (2000) 459-505.

(38) H.C. Jacqueline, G.I. Hong, Stretch effects on the burning velocity of turbulent premixed hydrogen/air flames, Proc. Combust. Inst. 28 (2000) 211-218.

(39) F.Dinkelacker, B.Manickam, S.P.R. Muppala, Modelling and simulation of lean premixed turbulent methane/hydrogen/air flames with an effective Lewis number approach, Combust. Flame 158 (2011) 1742-1749.

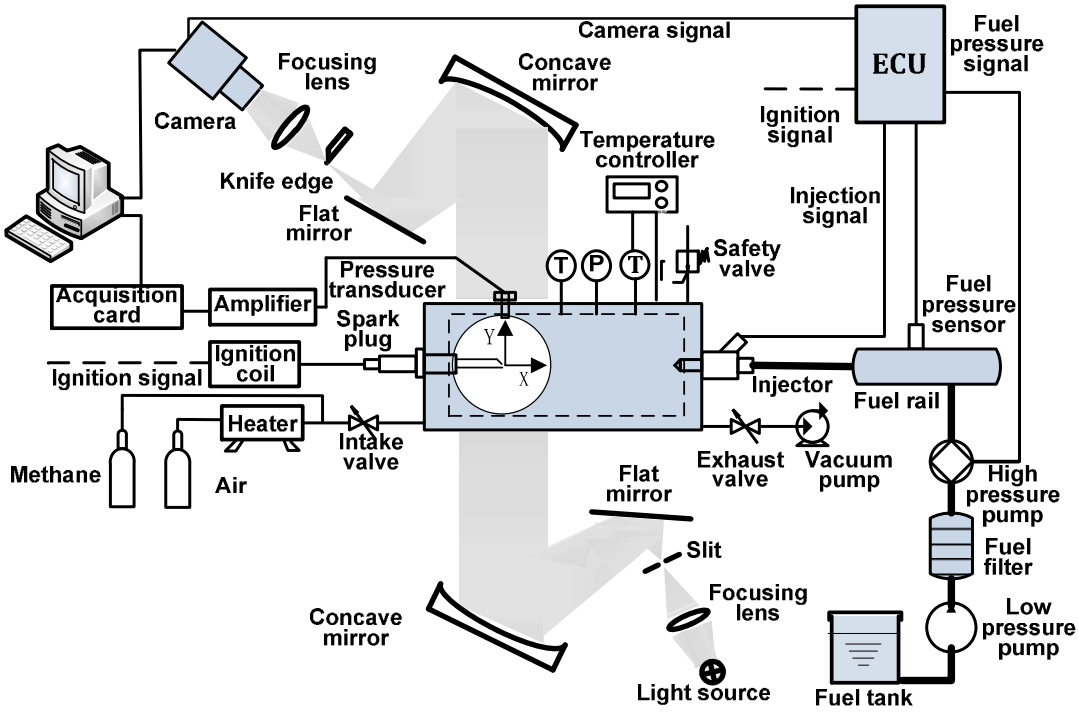

Figure 1. Schematic diagram of the experimental setup.

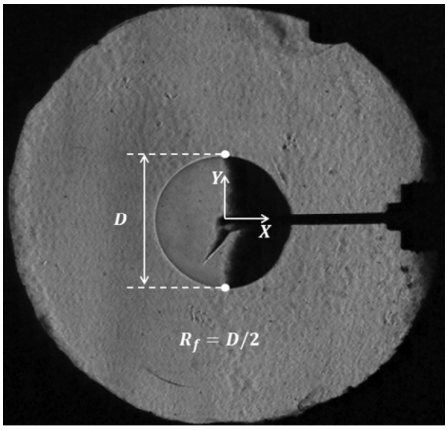

Figure 2. Flame Detection Technique.

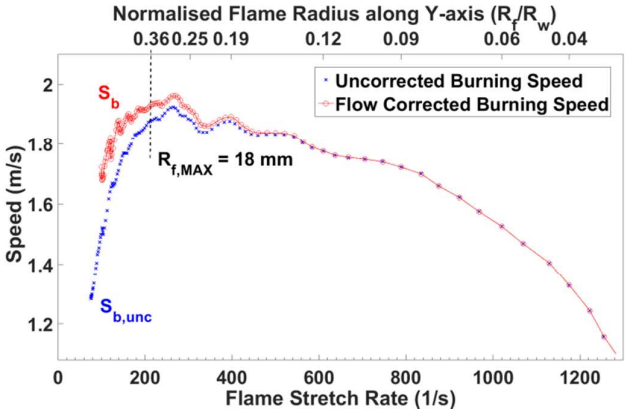

Figure 3. Illustration of Flow Correction Model for a stoichiometric PRF95-air mixture at $P_{initial}$=5 bar.

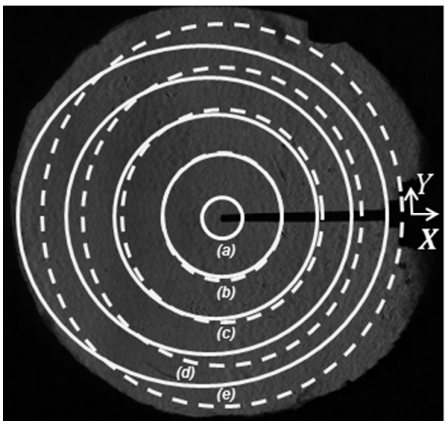

Figure 4. Symbolic illustration of flame surface contours for an unconfined (dotted lines) and cylindrically confined (solid lines) flame propagation process.

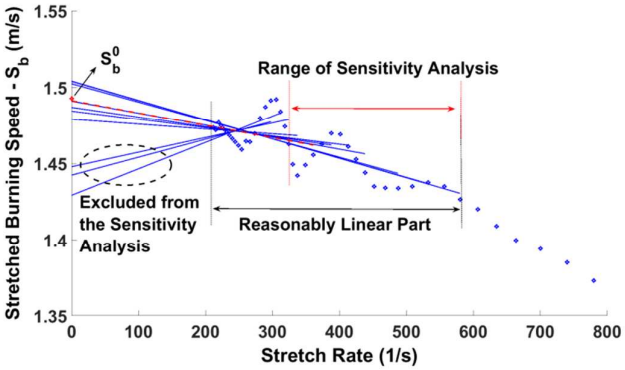

Figure 5. Definition of the Sensitivity Analysis.

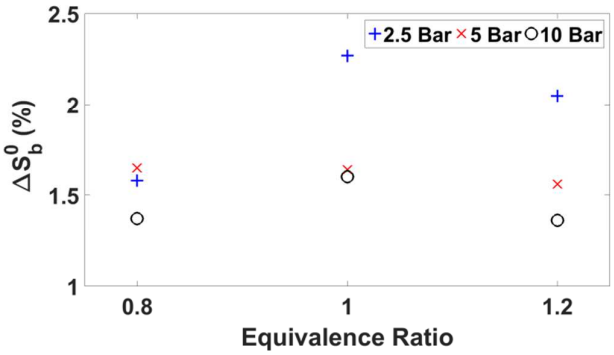

Figure 6. Induced uncertainty on S_b^0 due to the extrapolation technique.

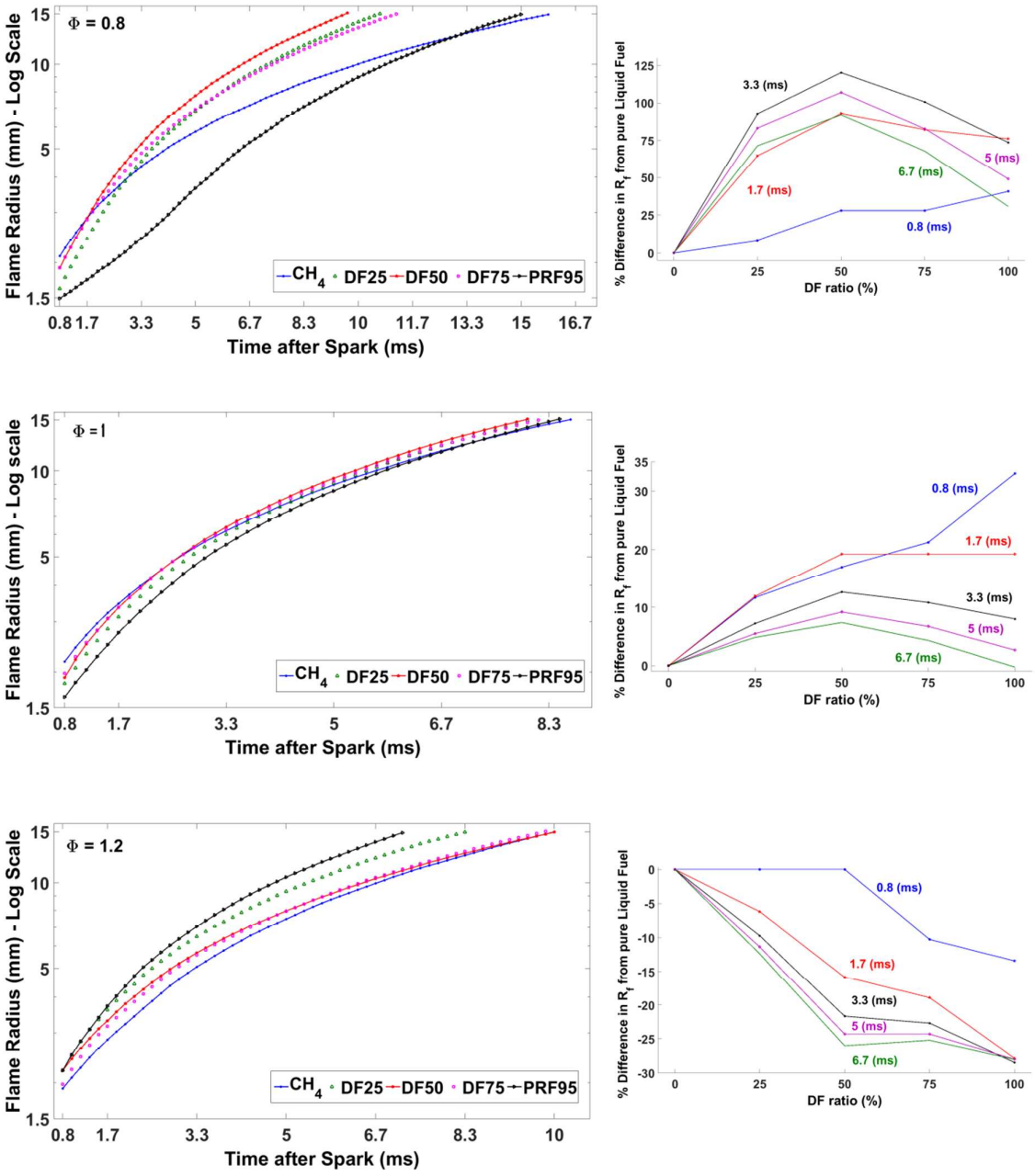

Figure 7. Flame Evolution of all fuels at $P_{initial}$ = 5Bar (Left plots). Sensitivity of the flame's radius to DF ratio (Right plots).

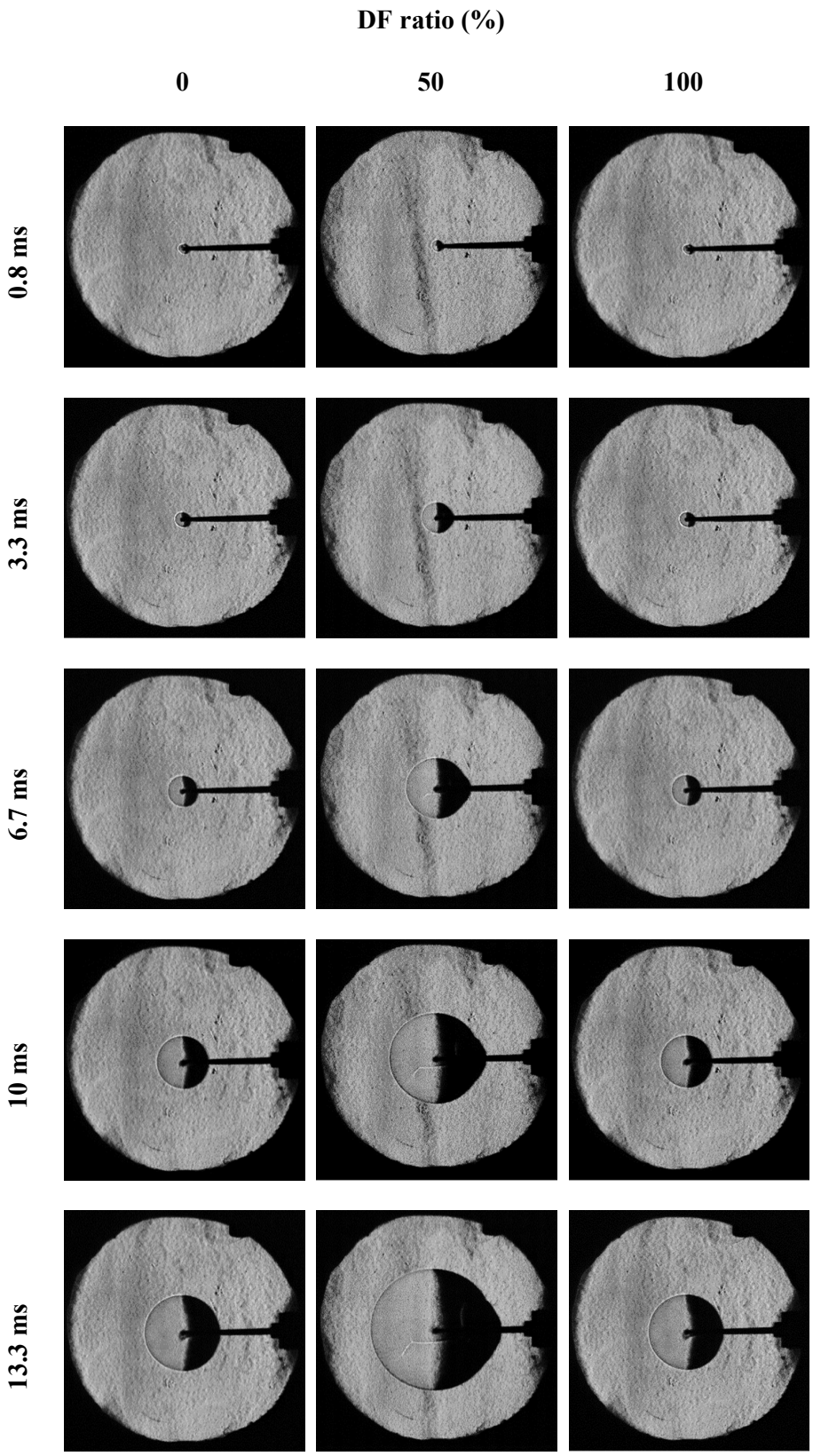

Figure 8. Chronological Schlieren Images at $\Phi = 0.8$, $P_{initial} = 5$Bar.

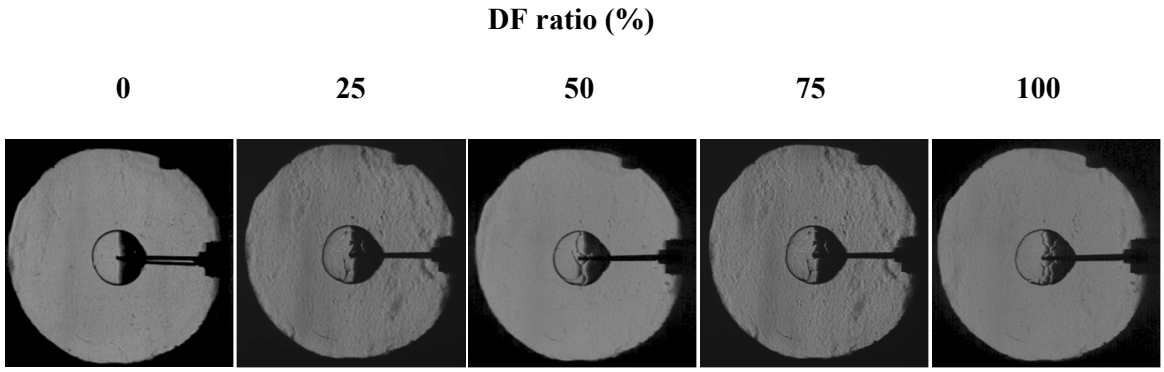

Figure 9. Schlieren Flame Images of all DF flames at Φ=1, $P_{initial}$ = 10 bar at a randomly selected Radius of 10mm.

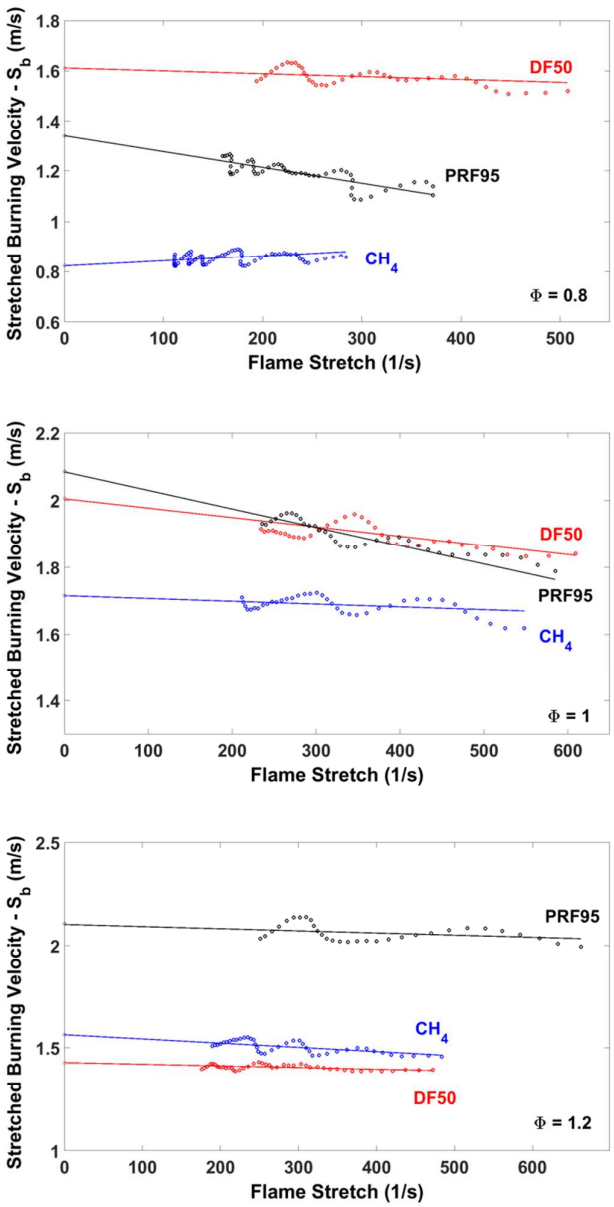

Figure 10. Stretched Burning Velocity versus Stretch Rate, $P_{initial}$: 5Bar.

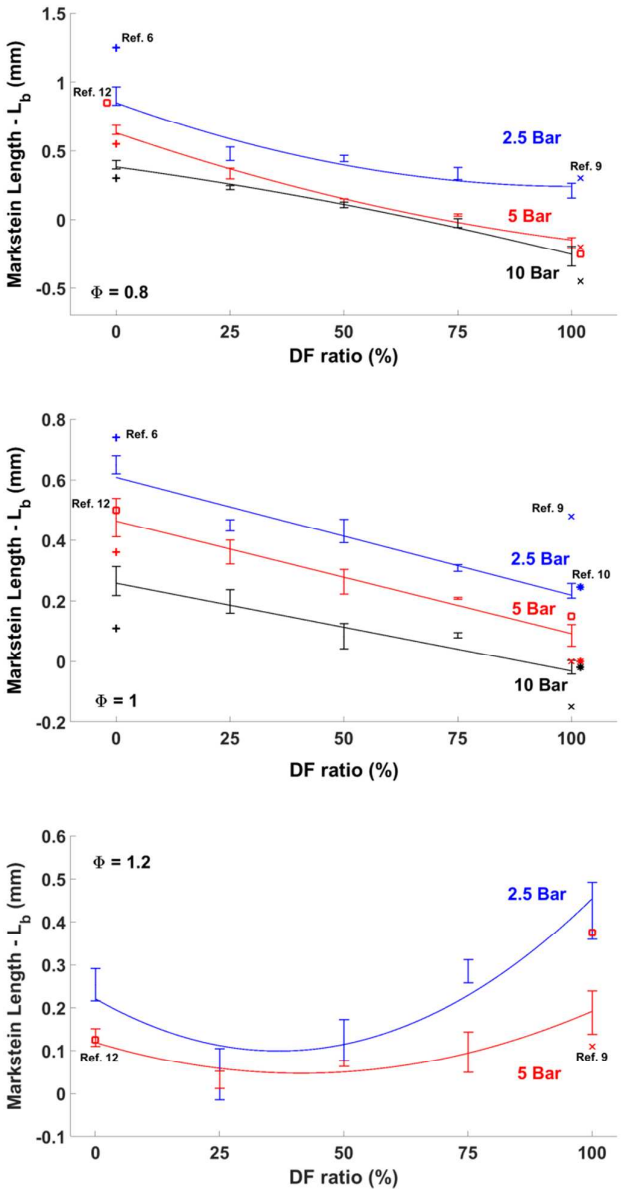

Figure 11. Burned Gas Markstein Length for all investigated conditions with available literature data.

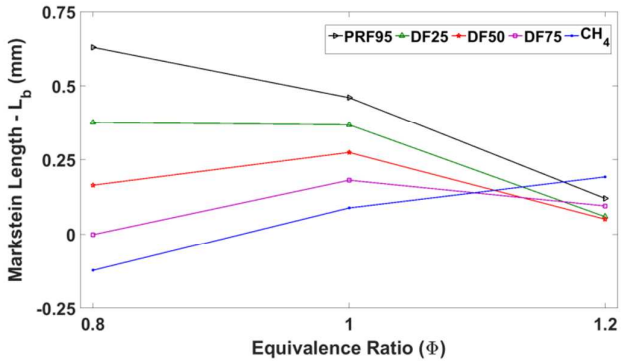

Figure 12. Markstein length versus Equivalence Ratio for all fuels at $P_{initial}$ = 5Bar.

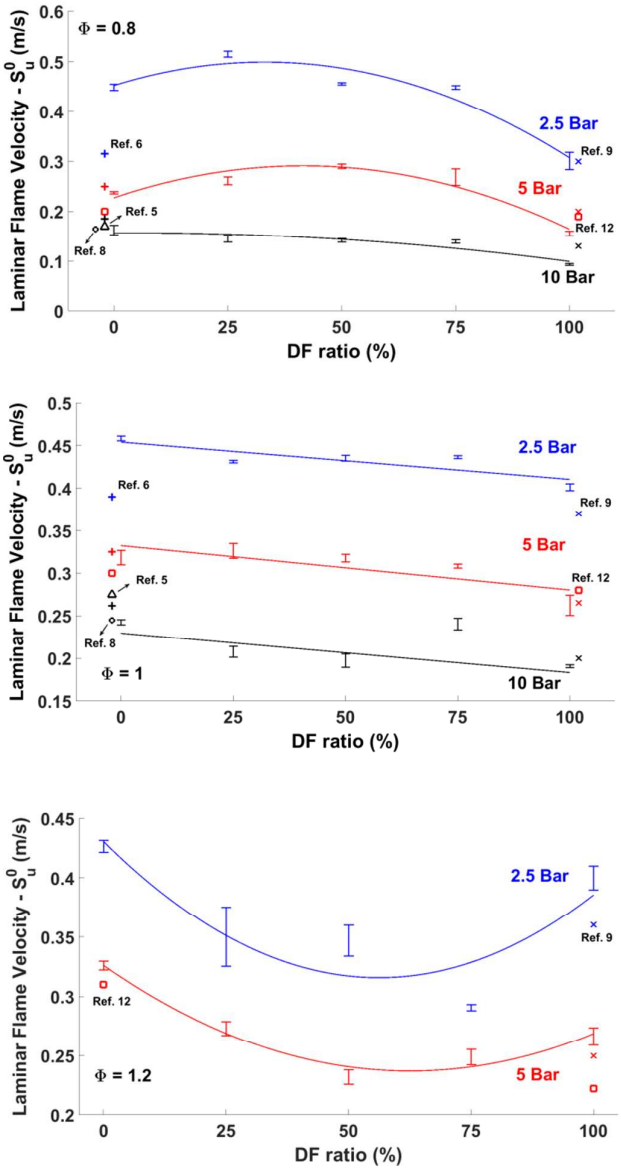

Figure 13 Laminar Flame Velocity for all investigated conditions with available literature data.

Fuel	CH_4 Mole Fraction	CH_4 Mass Fraction	Pressure (Bar)	Temperature (K)	Equivalence Ratio (Φ)
CH_4	1	1	2.5,5,10	373	0.8,1,1.2
DF75	0.95	0.728	2.5,5,10	373	0.8,1,1.2
DF50	0.86	0.470	2.5,5,10	373	0.8,1,1.2
DF25	0.68	0.228	2.5,5,10	373	0.8,1,1.2
PRF95	0	0	2.5,5,10	373	0.8,1,1.2

Table 1 : Summary of Experimental Conditions

Φ		***2.5Bar***	***5Bar***	***10Bar***
	a	5.92×10^{-5}	3.57×10^{-5}	-1.84×10^{-5}
0.8	*b*	-1.2×10^{-2}	-1.11×10^{-2}	-4.51×10^{-3}
	c	0.85	0.63	0.38
	a	-3.9×10^{-3}	-3.72×10^{-3}	-2.91×10^{-3}
1	*b*	0.61	0.46	0.26
	a	-8.91×10^{-5}	4.22×10^{-5}	
1.2	b	6.6×10^{-3}	-3.5×10^{-3}	-
	c	0.22	0.12	

Table 2. Fitting Coefficients for the trends in Markstein Length, L_b.

Φ		***2.5Bar***	***5Bar***	***10Bar***
	a	-4.31×10^{-5}	-3.71×10^{-5}	-6.33×10^{-5}
0.8	*b*	2.86×10^{-3}	3.08×10^{-3}	5.53×10^{-5}
	c	0.45	0.23	0.16
	a	-4.37×10^{-4}	-5.2×10^{-4}	-4.64×10^{-4}
1	*b*	0.45	0.33	0.23
	a	3.64×10^{-5}	2.27×10^{-5}	
1.2	*b*	-4.1×10^{-3}	-2.8×10^{-3}	-
	c	-0.43	-0.33	

Table 3. Fitting Coefficients for the trends in Laminar Flame Velocity, S_u^0.